Sociedade Brasileira de Automática (SBA)
IX Simpósio Brasileiro de Sistemas Elétricos - SBSE 2022, 10 a 13 de julho de 2022

Model Predictive Control for Voltage Regulation of Standalone Self-Excited Induction Generator

Gabriel M. Cocco * **Carlos A. de Souza** * **Felipe B. Grigoletto** **
Robinson F. de Camargo * **Fábio E. Bisogno** *

* *Power Electronics and Control Research Group, Federal University of Santa Maria, Santa Maria, RS, Brazil (e-mail: maiercocco@gmail.com, souza.engeeletrica@gmail.com, robinson.camargo@gmail.com, fbisogno@gmail.com).*
** *Energy Processing and Control Laboratory, Federal University of Pampa, Alegrete, RS, Brazil (e-mail: grigoletto@gmail.com).*

Abstract: This paper deals with a predictive current control strategy applied to voltage regulation in off-grid microgeneration systems based on self-excited induction generator (SEIG). A finite-control-set model predictive control (FCS-MPC) is used. This controller runs a discrete-time model to predict the future behavior of inverter currents for each switching state, then a control action is defined minimizing an appropriate cost function. Also combining proportional integral actions, the proposed control is capable of properly performing voltage regulation and harmonic compensation of positive, negative and zero sequence. The four-leg inverter is employed as DSTATCOM, this topology is a commonly used solution for powering standalone systems as it provides balanced three-phase voltages even under unbalanced load conditions. Simulations are presented to validate the proposed control technique, as well as to evaluate the performance of the system based on the IEEE 519-2014 and IEEE 1159-2009 Power Quality Standards.

Keywords: Active compensation, Predictive control, Induction generators, Voltage standards, Standalone system

1. INTRODUCTION

Electricity is essential for world production systems, as well as for the economic growth of nations. Ensuring a low-cost and reliable source of renewable energy is essential to meet energy demand of consumers today and in the future (IEA, 2021). The use of renewable energy sources, combined with distributed generation systems in micro-grid configurations, can be an alternative to reduce costs related to the installation of conventional transmission and distribution lines. In this way, Self-Excited Induction Generators (SEIGs) stand out, as isolated generation systems, based on water, wind or biomass potentials (Singh and Kasal, 2008).

The voltage regulation of the SEIG is directly related to the balance of reactive and active power of the AC bus. However, the SEIG is susceptible to load variations in the system, causing the changes of machine slip, which results in variation of reactive power and synchronous speed (Farret, 2010). In order to guarantee voltage regulation at the point of common coupling (PCC), several topologies for reactive power compensation have been proposed for the SEIG (Chauhan et al., 2010). Among these, the four-leg inverter, characterized as Distribution Static Synchronous Compensator (DSTATCOM), as proposed in Figure 1, stands out, due to its performance in voltage regulation and also in the compensation of reactive and harmonic components (Marra and Pomilio, 1999; Scherer et al., 2016; Grigoletto et al., 2019). Four-leg inverters are proven to be the best candidate to provide balanced voltages to linear, non-liner, balanced and unbalanced loads (Yaramasu et al., 2014; Pichan et al., 2017). The midpoint of the fourth leg provides the neutral point to the loads.

As a proposal of the DSTATCOM, in systems that present regulation problems, it is necessary specific control strategies that maintain regulated both the frequency and the amplitude of the voltages around the rated values suitable for the microgeneration system. Thus, to meet power quality standards, it is crucial to use control techniques that enable a fast dynamic response. Proportional Integral (PI) type controllers are presented in (Rai et al., 1993), however, they are not able to compensate for current harmonics, due to their limited bandwidth.

On the other hand, Proportional Resonant Controllers (PRs) are attractive because they are based on the principle of the internal model. These provide ideally infinite gain at chosen frequencies, ensuring tracking of sinusoidal references, rejecting disturbances and reducing harmonics at specific frequencies (Cocco et al., 2020). However, in cases of critical load conditions for a microgeneration system, it is necessary to use PRs at various frequencies of interest, so that they reject high and low order harmonics and, therefore, causing the reduction of the passband,

⋆ This work was supported in part by the Coordenação de Aperfeiçoamento de Pessoal de Nível Superior - Brasil (CAPES/PROEX) - Finance Code 001, and in part by INCT-GD and its funding agencies (CNPq process nº 465640/2014-1, CAPES process nº 23038.000776/2017-54 and FAPERGS process nº 17/2551-0000517-1).

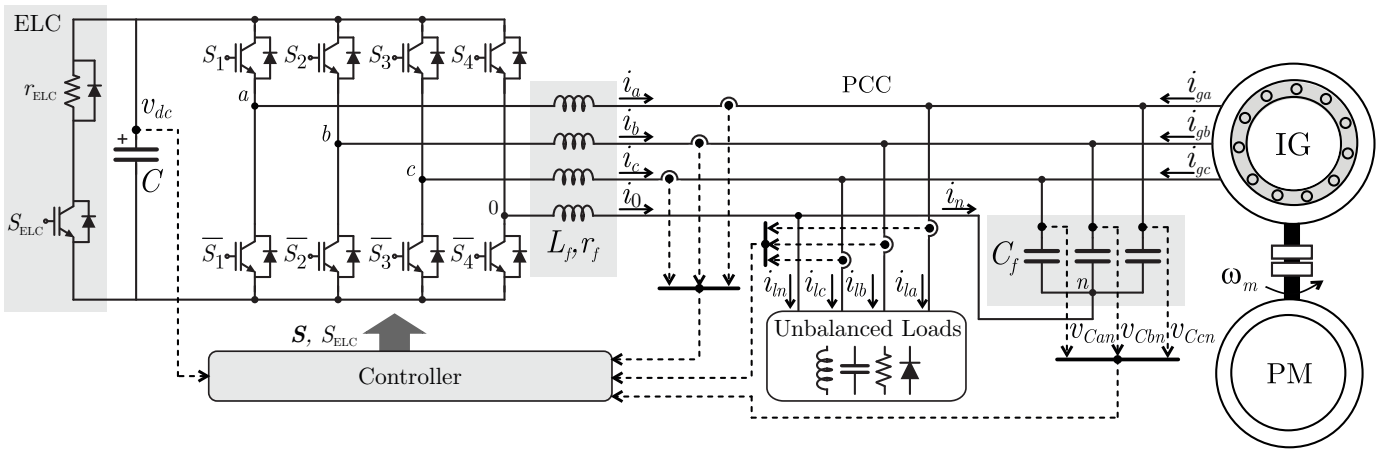

Figure 1. Diagram of the microgeneration system.

decreasing the fast dynamic response and even causing instability in the control of the system.

To improve the performance of the microgeneration system, a Model Predictive Control (MPC) is presented, considered as an algorithm that uses the system model to predict its future behavior and selects the most appropriate control action based on an optimization criterion Kouro et al. (2009). The predictive controller has been widely applied to power electronics, proving to be attractive due to its faster dynamic response, surpassing classical controllers, both PIs and PRs (Vazquez et al., 2017; Rivera et al., 2013a). MPC has been used in four-leg converters (Rodriguez et al., 2010; Rivera et al., 2013b; Yaramasu et al., 2014). The main advantage of using this type of controller is that it can easily handle constraints in the control loop, for example, saturation, switching frequency and power losses. MPC for Power Electronics can be described by two main categories, continuous control set (CCS-MPC) and finite control set (FCS-MPC).

The CCS-MPC has the main advantage of using a continuous control signal together with a PWM modulator that provides a fixed switching frequency, simplifying the power filter design (Judewicz et al., 2016). The tradeoff is a slight reduction on the dynamic response. Furthermore, this approach has the advantage that, for an unconstrained optimization problem, the solution can be analytically obtained offline. However, it can be mathematically complex, especially with the addition of constraints. On the other hand, among the several approaches, the FCS-MPC makes use of the inherent discrete nature of power converters (Kouro et al., 2009). Since they have a finite number of switching states, the optimization problem is limited to predict the system behaviour for those possible switching states over a short horizon. A constraint of MPC is that without a modulator the switching frequency is not enforced to be constant.

In this sense, this paper proposes FSC-MPC associated to PI controllers applied to the compensation of unbalances and zero-sequence harmonics caused by nonlinear single-phase loads in four-wire standalone microgeneration systems. The microgeneration system is based on a self-excited induction generator, also consisting of a DSTATCOM and three-phase and single-phase linear and nonlinear loads to perform the analysis. The proposed controller seeks to achieve good performance and present a simple design solution, exploring the capability of microcontroller technology. Simulation results are presented in order to validate the proposed control strategy, as well as to evaluate the system performance in terms of standards related to power quality, according to IEEE 519-2014, for voltage harmonics and the IEEE 1159-2009, under unbalanced load conditions.

2. SYSTEM DESCRIPTION AND MODELING

From the diagram shown in Figure 1, in order to modeling the four-wire microgeneration system, some simplifications were assumed, such as the steady-state equivalent Induction Generator (IG) circuit, which resembles an ideal transformer as shown in Figure 2. The complete IG circuit features two electrical circuits coupled by a magnetic field, which transfers energy from one circuit to another. The transformation ratio between the coils (stator and rotor), is considered unitary for an IG, so the voltage induced in the rotor is equal to the voltage induced in the stator, $v_r = v_{g(a,b,c)}$. It is possible to apply Thévenin theorem to the IG circuit, representing the steady state condition. Taking these conditions, the Thévenin impedance Z is obtained from Figure 2 (a) based on a single-phase circuit that can be reproduced for a three-phase circuit (b).

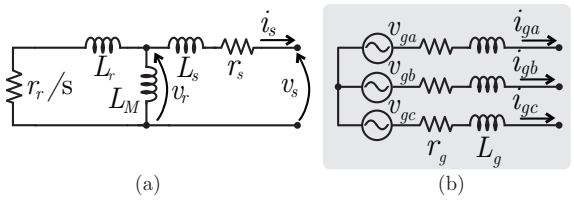

Figure 2. (a) Equivalent circuit per phase (b) Resulting three-phase.

Thévenin impedance can be written as:

$$Z = \frac{j\omega L_M \left(r_r/\mathrm{s} + j\omega L_r\right)}{j\omega L_M + \left(r_r/\mathrm{s} + j\omega L_r\right)} + r_s + j\omega L_s, \qquad (1)$$

where ω is the electrical frequency.

The impedance Z is composed of the stator resistance, rotor resistance (r_s, r_r, respectively), stator, rotor and mu-

tual inductances (L_s, L_r, L_M, respectively), rotor voltage (v_r) and slip coefficient (s). In order to find the circuit parameters for the system modeling, the complex portion of (1) is separated into a real part, corresponding to resistance (r_g), given by:

$$r_g = r_s + (r_r/\mathrm{s})\left(\frac{{L_M}^2}{(r_r/\mathrm{s})^2 + (L_M + L_r)^2}\right). \quad (2)$$

In addition, an imaginary part corresponding to an inductance (L_g), is given by:

$$L_g = \frac{(r_r/\mathrm{s})^2(L_M + L_s) + {L_M}^2 {L_r}^2 + L_s(L_M + L_r)^2}{(R_r/\mathrm{s})^2 + (L_M + L_r)^2}. \quad (3)$$

Figure 3 presents the equivalent model of the three-phase four-wire circuit of the microgeneration system shown in Figure 1 and the simplified IG model shown in Figure 2 (b).

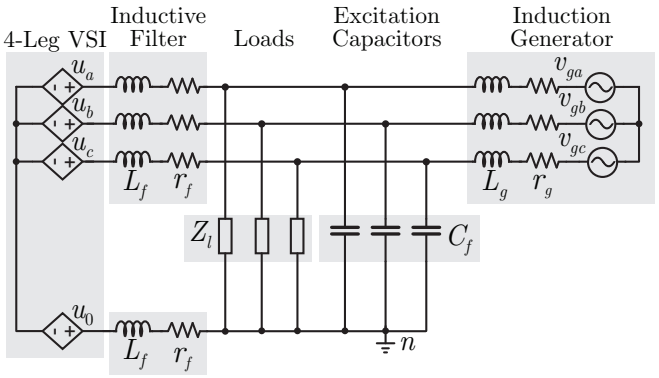

Figure 3. Equivalent circuit model.

Therefore, some simplifications were adopted, such as the dc link voltage, v_{dc}, represented as a constant dc source, the DSTATCOM switches are considered ideal, the output filter inductances are identicals, the switching frequency is greater than the fundamental frequency of the PCC voltages and finally, DSTATCOM is replaced by a voltage source representing its average value. Thereby, it is obtained a set of state-space equations of the microgeneration system in stationary coordinates, which are represented by:

$$\dot{\mathbf{x}}_{\alpha\beta0}(t) = \mathbf{A}_{\alpha\beta0}\mathbf{x}_{\alpha\beta0}(t) + \mathbf{B}_{\alpha\beta0}\mathbf{u}_{\alpha\beta0}(t) + \mathbf{F}_{\alpha\beta0}\mathbf{w}_{\alpha\beta0}(t), \quad (4)$$

where the state variables are given by:

$$\mathbf{x}_{\alpha\beta0}(t) = [i_{g\alpha}\ i_{g\beta}\ i_{g0}\ v_{C\alpha}\ v_{C\beta}\ v_{C0}\ i_\alpha\ i_\beta\ i_0]^\top, \quad (5)$$

the three-phase voltage control input variables are $\mathbf{u}_{\alpha\beta0} = [u_\alpha\ u_\beta\ u_0]^\top$ and the disturbance inputs are $\mathbf{w}_{\alpha\beta0} = [v_{g\alpha}\ v_{g\beta}\ v_{g0}]^\top$. Finally, the state-space matrices are given by (6).

$$\mathbf{A}_{\alpha\beta0} = \begin{bmatrix} \mathbf{I}_{3\times3}(-r_g/L_g) & \mathbf{A}_{p1}(-1/L_g) & \mathbf{0}_{3\times3} \\ \mathbf{I}_{3\times3}(1/C_f) & \mathbf{I}_{3\times3}(-1/C_f Z_l) & \mathbf{I}_{3\times3}(1/C_f) \\ \mathbf{0}_{3\times3} & \mathbf{A}_{p2}(-1/L_f) & \mathbf{I}_{3\times3}(-r_f/L_f) \end{bmatrix};$$
$$\mathbf{B}_{\alpha\beta0} = \begin{bmatrix} \mathbf{0}_{3\times3} \\ \mathbf{0}_{3\times3} \\ \mathbf{A}_{p2}(1/L_f) \end{bmatrix},\ \mathbf{F}_{\alpha\beta0} = \begin{bmatrix} \mathbf{A}_{p1}(1/L_g) \\ \mathbf{0}_{3\times3} \\ \mathbf{0}_{3\times3} \end{bmatrix}. \quad (6)$$

where C_f is the equivalent excitation capacitance, Z_l is the load impedance, L_f and r_f are the inductance and resistance of the inductive filter, the Thevénin equivalent inductance and resistance for the generator model are L_g and r_g, respectively.

The sinusoidal components in $\alpha\beta0$ can be expressed in synchronous coordinates $dq0$. Hereupon, the state-space equations can be represented by:

$$\dot{\mathbf{x}}_{dq0}(t) = \mathbf{A}_{dq0}\mathbf{x}_{dq0}(t) + \mathbf{B}_{dq0}\mathbf{u}_{dq0}(t) + \mathbf{F}_{dq0}\mathbf{w}_{dq0}(t), \quad (7)$$

where state variables in synchronous coordinates are given by:

$$\mathbf{x}_{dq0}(t) = [i_{gd}\ i_{gq}\ i_{g0}\ v_{Cd}\ v_{Cq}\ v_{C0}\ i_d\ i_q\ i_0]^\top, \quad (8)$$

the control variables are represented by $\mathbf{u}_{dq0} = [u_d\ u_q\ u_0]^\top$ and the disturbance variables are $\mathbf{w}_{dq0} = [v_{gd}\ v_{gq}\ v_{g0}]^\top$, finally the matrices are represented by:

$$\mathbf{A}_{dq0} = \begin{bmatrix} \mathbf{A}_{p3} & \mathbf{A}_{p1}(-1/L_g) & \mathbf{0}_{3\times3} \\ \mathbf{I}_{3\times3}(1/C_f) & \mathbf{A}_{p4} & \mathbf{I}_{3\times3}(1/C_f) \\ \mathbf{0}_{3\times3} & \mathbf{A}_{p2}(-1/L_f) & \mathbf{A}_{p5} \end{bmatrix};$$
$$\mathbf{B}_{dq0} = \begin{bmatrix} \mathbf{0}_{3\times3} \\ \mathbf{0}_{3\times3} \\ \mathbf{A}_{p2}(1/L_f) \end{bmatrix},\ \mathbf{F}_{dq0} = \begin{bmatrix} \mathbf{A}_1(1/L_g) \\ \mathbf{0}_{3\times3} \\ \mathbf{0}_{3\times3} \end{bmatrix}. \quad (9)$$

where the coefficients correspond to the following matrices:

$$\mathbf{A}_{p1} = \begin{bmatrix} 1 & 0 & 0 \\ 0 & 1 & 0 \\ 0 & 0 & 0 \end{bmatrix},\ \mathbf{A}_{p2} = \begin{bmatrix} 1 & 0 & 0 \\ 0 & 1 & 0 \\ 0 & 0 & 1/4 \end{bmatrix};$$
$$\mathbf{A}_{p3} = \begin{bmatrix} -r_g/L_g & \omega & 0 \\ -\omega & -r_g/L_g & 0 \\ 0 & 0 & -r_g/L_g \end{bmatrix};$$
$$\mathbf{A}_{p4} = \begin{bmatrix} -1/C_f Z_l & \omega & 0 \\ -\omega & -1/C_f Z_l & 0 \\ 0 & 0 & -1/C_f Z_l \end{bmatrix};$$
$$\mathbf{A}_{p5} = \begin{bmatrix} -r_f/L_f & \omega & 0 \\ -\omega & -r_f/L_f & 0 \\ 0 & 0 & -r_f/L_f \end{bmatrix}, \quad (10)$$

where ω is a coupling coefficient.

The models obtained in $\alpha\beta0$ and $dq0$ frames are used to derive the transfer functions, in order to design a multi-loop control system. In this way, the inner control loops in $\alpha\beta0$ frame are used to control DSTATCOM currents. The outer control loops are intended to regulate both the PCC voltage and the dc bus voltage of the DSTATCOM in $dq0$ frame, where control become tracking a continuous signal, and a PI action can be employed with good performance. In order to design the outer loops, the controllers was carried out in the frequency domain. Nonetheless, for the inner loops, a discrete model of inverter output induction filter is used to control the currents in $\alpha\beta0$ frame.

2.1 PCC voltages modeling

For the outer loops, analyzing the ac voltage loop, in the synchronous frame $dq0$, the variable i_q is the current generated by the DSTATCOM, related to quadrature axis. Hereafter, a relationship between the output voltage v_{Cd} and i_q needs to be obtained, due to the synchronous orientation ($dq0$), given by $G_{v_{Cd}}$. In (11) the transfer function that relates the input current i_0 with the output voltage v_{C0} is given by $G_{v_{C0}}$. The main goal in controlling v_0 is to compensate for voltage unbalances since the

neutral currents are reflected to this axis, the transfer function that represents this loop is given by:

$$Gv_{Cd}(s), Gv_{C0}(s) = \mathbf{C}_{dq0}(s\mathbf{I} - \mathbf{A}_{dq0})^{-1}\mathbf{B}_{dq0};$$
$$Gv_{Cd}(s) = \frac{G_{v_{Cd},u_d}(s)}{G_{i_q,u_d}(s)},\ Gv_{C0}(s) = \frac{G_{v_{C0},u_0}(s)}{G_{i_0,u_0}(s)}, \quad (11)$$

where $\mathbf{C}_d = [0\,0\,0\,1\,0\,0\,0\,0\,0]$, $\mathbf{C}_q = [0\,0\,0\,0\,0\,1\,0\,0\,0]$ e $\mathbf{C}_0 = [0\,0\,0\,0\,0\,0\,1\,0\,0\,0]$.

2.2 Dc bus capacitor modeling

For the dc-link voltage control, a transfer function is obtained that relates the dc link voltage v_{dc} with the direct axis current i_d (Cocco et al., 2020). Thereby, the power flow analysis is performed applying the Tellegen theorem to obtain the dynamic model. Thus, $P_{dc_{bus}} = -P_{\text{ELC}} - P_{ac_{bus}}$, where the losses can be neglected. Assuming that $v_{Cq} = 0$, due to the transformation of stationary to synchronous frame, the power balance equation can be written as:

$$-v_{dc}C\frac{dv_{dc}}{dt} = \frac{(v_{dc}u_{\text{ELC}})^2}{r_{\text{ELC}}} + v_{Cd}i_d. \quad (12)$$

By applying the Laplace transform in (12), and applying the linearization and perturbation technique where $v_{dc}(t) = \tilde{v}_{dc}(t) + V_{dc}$ and $i_d(t) = \tilde{i}_d(t) + I_d$ results in:

$$G_{v_{dc}}(s) = \frac{v_{dc}(s)}{i_d(s)} = \frac{-V_{Cd}}{CV_{dc}\left(s + \frac{2{u_{\text{ELC}}}^2}{C\,r_{\text{ELC}}}\right)}. \quad (13)$$

2.3 Inverter currents modeling

Table 1 shows the sixteen switching states of the power converter presented in Figure 1. Each state corresponds to one output voltage vector in *abc* coordinates. These output voltage vectors can be is represented in $\alpha\beta0$ by means of the Clarke power invariant transformation.

From the system model obteined, the inverter is connected to PCC, the dynamics of the output currents in $\alpha\beta0$ can be written as:

$$\dot{\mathbf{i}}_{\alpha\beta0}(t) = \mathbf{A}\mathbf{i}_{\alpha\beta0}(t) + \mathbf{B}\left(\mathbf{u}_{\alpha\beta0}(t) - \mathbf{v}_{\alpha\beta0}(t)\right), \quad (14)$$

where,

$$\mathbf{A} = \begin{bmatrix} -R_f/L_f & 0 & 0 \\ 0 & -R_f/L_f & 0 \\ 0 & 0 & -R_f/L_f \end{bmatrix};$$
$$\mathbf{B} = \begin{bmatrix} 1/L_f & 0 & 0 \\ 0 & 1/L_f & 0 \\ 0 & 0 & 1/4L_f \end{bmatrix}, \quad (15)$$

$\mathbf{v}_{\alpha\beta0} = [v_{C\alpha} \quad v_{C\beta} \quad v_{C0}]^\top$ are grid voltages, and $\mathbf{u}_{\alpha\beta0(k)}$ are the inverter output voltages in $\alpha\beta0$ coordinates.

A discrete time form of (14) for a sampling time T_s can be used to predict the future value of the output current by:

$$\mathbf{i}^p_{\alpha\beta0(k+1)} = (\mathbf{I} + \mathbf{A}T_s)\,\mathbf{i}_{\alpha\beta0(k)} + \mathbf{B}T_s\left(\mathbf{u}_{\alpha\beta0(k)} - \mathbf{v}_{\alpha\beta0(k)}\right). \quad (16)$$

Moreover, a unit delay can be included to compensate for the implementation time of the microprocessor, according to Cortes et al. (2012); Kukrer (1996), using steps ahead in the prediction horizon and Lagrange extrapolation techniques in the reference variables. As the frequency of $\mathbf{v}_{\alpha\beta0}$ and $\mathbf{i}_{\alpha\beta0}$ are much smaller than the sampling frequency, it can be assumed that $\mathbf{v}^*_{\alpha\beta0(k)} \approx \mathbf{v}^*_{\alpha\beta0(k+1)}$ and $\mathbf{i}^*_{\alpha\beta0(k)} \approx \mathbf{i}^*_{\alpha\beta0(k+1)}$.

Table 1. Switching states and output voltages.

Vector	**Switching State**				**Output Voltage**		
j	S_1	S_2	S_3	S_4	u_α	u_β	u_0
1	0	0	0	0	0	0	0
2	0	0	0	1	0	0	$-\sqrt{3}v_{dc}$
3	0	0	1	0	$-\sqrt{\frac{2}{3}}v_{dc}/2$	$-v_{dc}/\sqrt{2}$	$v_{dc}/\sqrt{3}$
4	0	0	1	1	$-\sqrt{\frac{2}{3}}v_{dc}/2$	$-v_{dc}/\sqrt{2}$	$-2v_{dc}/\sqrt{3}$
5	0	1	0	0	$-\sqrt{\frac{2}{3}}v_{dc}/2$	$v_{dc}/\sqrt{2}$	$v_{dc}/\sqrt{3}$
6	0	1	0	1	$-\sqrt{\frac{2}{3}}v_{dc}/2$	$v_{dc}/\sqrt{2}$	$-2v_{dc}/\sqrt{3}$
7	0	1	1	0	$-\sqrt{\frac{2}{3}}v_{dc}$	0	$2v_{dc}/\sqrt{3}$
8	0	1	1	1	$-\sqrt{\frac{2}{3}}v_{dc}$	0	$-v_{dc}/\sqrt{3}$
9	1	0	0	0	$\sqrt{\frac{2}{3}}v_{dc}$	0	$v_{dc}/\sqrt{3}$
10	1	0	0	1	$\sqrt{\frac{2}{3}}v_{dc}$	0	$-2v_{dc}/\sqrt{3}$
11	1	0	1	0	$\sqrt{\frac{2}{3}}v_{dc}/2$	$-v_{dc}/\sqrt{2}$	$2v_{dc}/\sqrt{3}$
12	1	0	1	1	$\sqrt{\frac{2}{3}}v_{dc}/2$	$-v_{dc}/\sqrt{2}$	$-v_{dc}/\sqrt{3}$
13	1	1	0	0	$\sqrt{\frac{2}{3}}v_{dc}/2$	$v_{dc}/\sqrt{2}$	$2v_{dc}/\sqrt{3}$
14	1	1	0	1	$\sqrt{\frac{2}{3}}v_{dc}/2$	$v_{dc}/\sqrt{2}$	$-v_{dc}/\sqrt{3}$
15	1	1	1	0	0	0	$\sqrt{3}v_{dc}$
16	1	1	1	1	0	0	0

3. CONTROLLERS

The synchronization method is based on the Kalman Filter, which consists of a structure that ensures high performance in transient and measurement noise rejection, generating the synchronism signals: sine and cosine. Moreover, for the control, the cross-coupling between d and q axis is neglected, thus the presented system is considered as two SISO systems, where there are independent control loops for the axis d and for the axis q. The applied control strategy is based on the multi-loop control system, shown in Figure 4.

The three outer controllers determine the current references on axes $dq0$ (i^*_d, i^*_q and i^*_0) related to the regulation of PCC voltages and also to the dc bus voltage. These quantities are transformed to $\alpha\beta0$ currents (i^*_α, i^*_β and i^*_0), for the predictive controller, responsible for controlling the currents processed by DSTATCOM. Finally, these generate the switching state as a control action, direct for the IGBTs, in this case.

3.1 Outer control loops

The outer control loops generate the current references to be processed by DSTATCOM, in order to maintain the system voltage levels with zero error in relation to the predefined references. Hereafter, there are three individual voltage control loops. The first loop is defined for PCC voltage control, performed by controlling the ac bus voltage on the d axis (v_{Cd}), the second loop plays the role

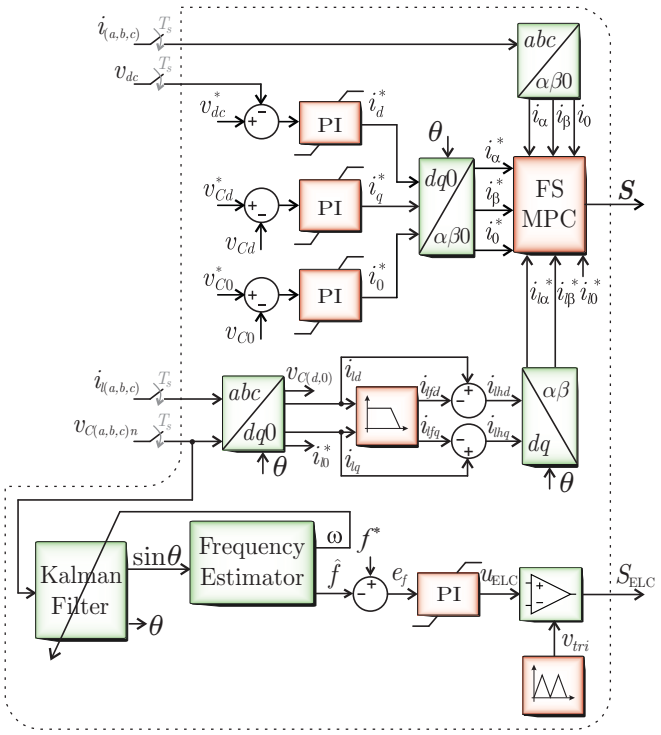

Figure 4. Four-wire three-phase multi-loop control system applied for DSTATCOM.

of dc bus voltage control (v_{dc}). On the other hand, the third loop controls the 0 axis (v_{C0}), seeking to correct possible harmonics and imbalances in the system currents and voltages, which is one of the main contributions of this work. If there are unbalances between the load currents i_{la}, i_{lb} and i_{lc} an alternating component appears in the current i_{l0}, causing imbalance in ac bus voltages, generating yet, an alternating component in voltage v_{C0}. The control of these voltage loops depends exclusively on the feedback of the system voltages, making it necessary to measure the PCC phase voltages and the dc-link voltage of the DSTATCOM.

Thereupon, proportional-integral controllers can be used to provide control of the outer loops. The controller generic expression in the discrete time domain is given by:

$$\begin{aligned} i^*_{(d,q,0)(k)} &= k_i x_{pi(k)} + k_p e_{v(k)}; \\ x_{pi(k+1)} &= x_{pi(k)} + T_s e_{v(k)}, \end{aligned} \tag{17}$$

where k_p and k_i are respectively the proportional and integral gain of the PI, and $e_{v(k)} = v^*_{(Cd,dc,0)(k)} - v_{(Cd,dc,0)(k)}$ is the outer loop voltages errors.

3.2 Model Predictive Control Description

The aim of MPC's is to predict the future behaviour of the variables over a period time called the horizon window. Therefore, an appropriate control action must be defined in order to drive these variables as close as possible to a desired reference values.

3.3 Cost Function Description

The discrete model of the system f_p is evaluated in order to predict the future values of $\mathbf{x}^p_{j(k+1)}$ for the possible control action $\mathbf{S}_j$, where:

$$\mathbf{x}^p_{j(k+1)} = f_p\left\{\mathbf{x}_{(k)}, \mathbf{S}_j\right\}, \quad \forall j \in \{1, ..., 16\}. \tag{18}$$

The vector $\mathbf{x}_{(k)}$ is composed of the measured inverter currents $\mathbf{i}_{\alpha\beta 0}$, that is $\mathbf{x}_{(k)} = \left[i_{\alpha(k)} \;\; i_{\beta(k)} \;\; i_{0(k)}\right]^\top$. Furthermore, f_g represents the discrete model (14) for the predicted output currents. There are sixteen possibilities for the cost function g_j, that is:

$$g_j = f_g\left\{\mathbf{x}^*, \mathbf{x}^p_j\right\}, \quad \forall j \in \{1, ..., 16\}. \tag{19}$$

It is important to point out that there are several ways to define a cost function which depends on the nature of the different terms involved in the formulation Cortes et al. (2009). A suitable cost function can be defined as:

$$g_j = (i^*_\alpha - i^p_{\alpha j})^2 + (i^*_\beta - i^p_{\beta j})^2 + (i^*_0 - i^p_{0j})^2, \tag{20}$$

Therefore the control action $\mathbf{S}_{(k+1)}$ that drives $\mathbf{x}$ as close as possible to the desired reference $\mathbf{x}^*$ must minimize the cost function f_g as

$$\mathbf{S}_{(k+1)} = \arg\left\{\min_{\mathbf{S}_j} f_g\left\{\mathbf{x}^*, \mathbf{x}^p_j(\mathbf{S}_j)\right\}\right\}, \quad \forall j \in \{1, ..., 16\}. \tag{21}$$

3.4 Frequency control and synchronization method

As considered in Scherer et al. (2016); Cocco et al. (2020), a hydro turbine operating above the synchronous speed is the prime mover, and the frequency control is performed by the ELC. The voltage frequency depends on the balance between input mechanical active power and output active power of the SEIG. Therefore, the power consumed by the system must be maintained constant irrespective of the load variations. The ELC is used to consume the surplus active power generated by the SEIG. On the other hand, energy storage systems can be considered and integrated, where energy can be reused during peak demand times.

The estimated PCC voltage frequency is performed by a Kalman-based synchronization method followed by a frequency identification algorithm. The estimated frequency ($\hat{f}$) is then compared with the reference value, which generates a frequency error, $e_f = f^* - \hat{f}$. The error feeds a PI controller which defines the power to be consumed by the ELC. The control action u_{ELC} is modulated to generate a PWM signal to be applied to the IGBT which drives the r_{ELC}.

4. SIMULATION RESULTS

In this section, simulation results are presented to validate the design methodology and structure of the controllers proposed for the microgeneration system. In this way, tests are carried out before and after the connection of linear and nonlinear balanced and unbalanced loads to the system, presenting interesting results that meet the energy quality standards. For that, the parameters considered for the simulation are respectively presented in Tables 2 and 3, the nominal values for the SEIG, the parameters of the inverter and the ELC.

To test the response of the inner loop current controllers, they can be analyzed considering the ability to track a reference under amplitude and phase variations. In

Table 2. SEIG parameters

Parameter	Value
Nominal power	P_n = 3.7 kW (5 cv)
Line voltage (RMS)	v'_s = 380 V
Nominal rotor speed	n = 1730 rpm
Frequecy	f = 60 Hz
Power factor	FP = 0.81
Excitation capacitor	C_f = 55 μF
Thévenin equivalent	L_g= 5 mH, r_g= 0.2 Ω

Table 3. Parameters of the inverter and ELC

Parameter	Value
Dc-link capacitor	C = 4700 μF
Output filter	L_f= 4 mH, r_f= 0.17 Ω
Sampling period	T_s = 25 μs
ELC resistor	r_{ELC} = 48 Ω - 4 kW

the outer voltage loops, only amplitude variations were applied. The step responses of the current controllers are shown in Figures 5 and 6. These Figures show a good transient response of the current controllers i_α, i_β and i_0. To obtain these results, the dc-link capacitor was replaced by a dc voltage source and a short-circuit experiment on the output inductor filter terminals is performed. Thus, variations on amplitude are applied to the current references and later 180° changes to the phase of the references are applied, separately for each axis i^*_α, i^*_β and i^*_0. Thus, the FS-MPC control strategy, applied to the inner loops, has the ability to offer the microgeneration system a fast dynamic response.

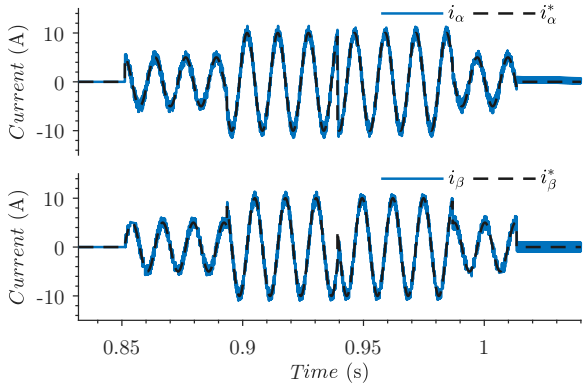

Figure 5. Reference traking of i_α, i_β current loops.

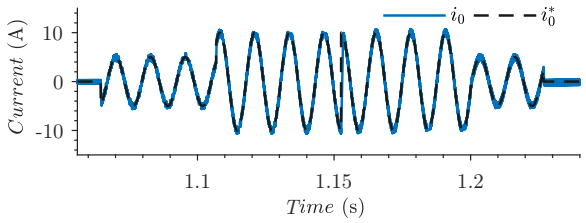

Figure 6. Reference traking of i_0 current loop.

Figures 7, 8 and 9 respectively, present the transient response of the controllers of the external voltage loops, the inverter dc-link, the PCC voltages on the d axis and the PCC voltages on the 0 axis. In this case, there is a variation in the signal of the voltage reference v^*_{dc} from 650 V to 600 V, in the v^*_{Cd} from 380 V to 320 V, and finally in the v^*_0 is applied from 0 V to 100 V. With this, it is possible to observe that the voltage loops have proper tracking for the submitted reference signal.

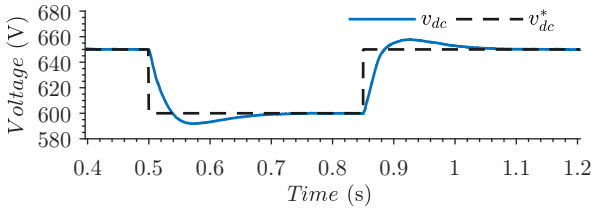

Figure 7. Step response for the dc-link voltage.

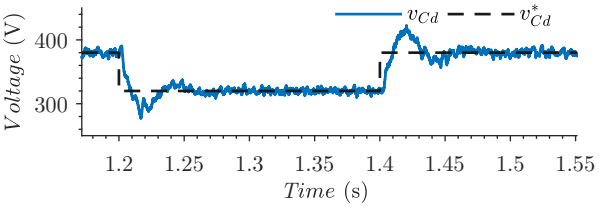

Figure 8. Step response for the PCC voltages.

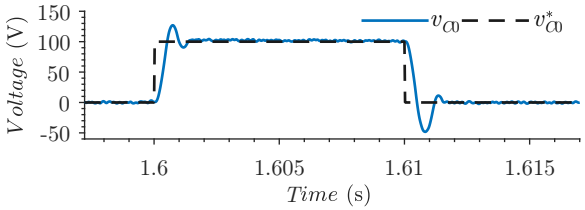

Figure 9. Step response for the zero-axis voltage.

Through the FS-MPC control strategy applied to the microgeneration system, it must maintain the frequency and voltages regulated around the nominal values, even under unbalanced load conditions, also keeping the voltage THD below the levels established by the IEEE power quality standards.

Figure 10 presents the dynamic performance of the designed current controller, when is connected to the system a 1 kW single-phase nonlinear load in phase c of the system, showing the tracking of the reference imposed by the dynamics of the load currents. It is verified the fast dynamic response of the FS-MPC controller for the current tracking under the tested load.

Figure 11 shows the tracking for the currents i_α, i_β and i_0 for a 3.2 kW balanced nonlinear load. In this way, controllers present the ability to quickly trace the references imposed by the load on $i_\alpha{}^*$ and $i_\beta{}^*$. Reference $i_0{}^*$ remains null due to the characteristic of a balanced three-phase system without zero-sequence components.

Figure 12 shows the simulation results of the microgeneration system under the connection of three-phase and single-phase loads, showing the performance of the system variables through load transients. Figure 12(a) presents the nature of the loads applied at each instant of the simulation, presenting the active and reactive powers of the load. Active and reactive powers processed by the inverter

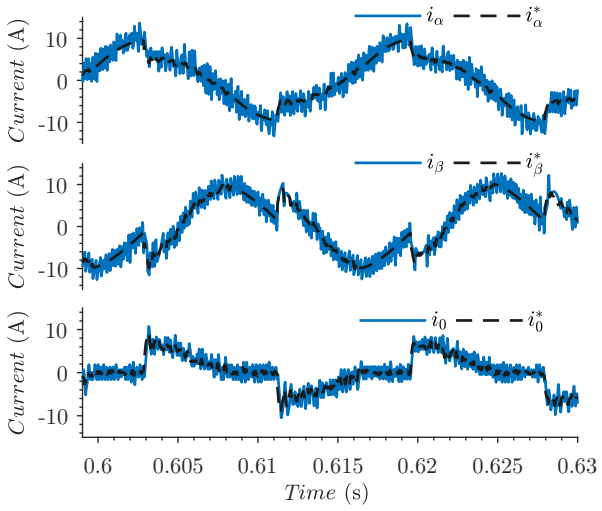

Figure 10. Reference traking of currents under unbalanced nonlinear load (1 kW).

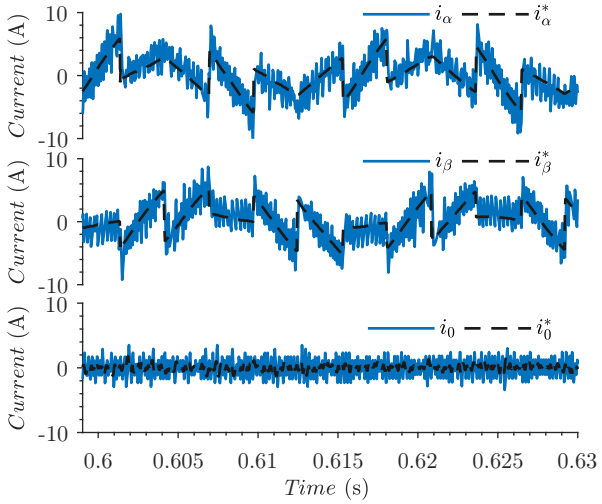

Figure 11. Reference traking of currents under balanced nonlinear load (3,2 kW).

can be seen in Figure 12(b). Figure 12(c) presents the RMS line voltages on the PCC, Figure 12(d) shows the voltage on the dc-link capacitor, Figure 12(e) presents the frequency of the voltages on the PCC and Figure 12(f) the voltage and current on axis 0. Also, it can be verified through an analysis of the harmonic content of the PCC voltages in Figure 12(g), the control performance under the system, presenting a THD below the limit of 8 % established by the IEEE 519-2014 standard. At the instant 1.8 s, THD exceeds the IEEE limit due to a transient response. However, it is within the tolerance allowed by the standard. It is also possible to verify that the unbalance caused to the system under all imposed load conditions remains in compliance with the limit of 2 % established by the IEEE 1159-2009 standard according to Figure 12 (h).

5. CONCLUSION

This paper presented the development of a combined control strategy, using predictive controllers for SEIG voltage regulation and harmonic compensation, in a four-wire standalone microgeneration system. PI controllers are employed to the outer voltage loops.

Simulation results validated the proposed control system for the voltage and current loops. These results showed an adequate transient response for the control, allowing to verify, through a THD analysis, a reduction in the harmonic content, present in the PCC voltages, meeting the recommendations of IEEE 519-2014, for voltage harmonics. In this way, the performance of the voltage loop v_0, for unbalances control, remains below the limits imposed by IEEE 1159-2009 under single-phase nonlinear load conditions.

REFERENCES

Chauhan, Y.K., Jain, S.K., and Singh, B. (2010). A prospective on voltage regulation of self-excited induction generators for industry applications. *IEEE Transactions on Industry Applications*, 46(2), 720–730.

Cocco, G.M., Scherer, L.G., Grigoletto, F.B., and de Camargo, R.F. (2020). Proportional-resonant controller applied to dstatcom in a hybrid hydro-pv generation system. In *Congresso Brasileiro de Automática-CBA*, volume 2.

Cortes, P., Kouro, S., Rocca, B.L., Vargas, R., Rodriguez, J., Leon, J.I., Vazquez, S., and Franquelo, L.G. (2009). Guidelines for weighting factors design in model predictive control of power converters and drives. In *2009 IEEE Intern. Conf. on Ind. Tech.*, 1–7.

Cortes, P., Rodriguez, J., Silva, C., and Flores, A. (2012). Delay compensation in model predictive current control of a three-phase inverter. *IEEE Trans. on Ind. Electron.*, 59(2), 1323–1325.

Farret, F.A. (2010). *Harnessing Small Sources of Electricity*. Federal University of Santa Maria, 1nd edition.

Grigoletto, F.B., Cocco, G.M., Scherer, L.G., and de Camargo, R.F. (2019). Control of three-phase four-wire ssi dstatcom integrated to pv generation system. In *2019 IEEE PES Innovative Smart Grid Technologies Conference - Latin America (ISGT Latin America)*, 1–6.

IEA, I.E.A. (2021). Global energy review 2021 assessing the effects of economic recoveries on global energy demand and co2 emissions in 2021. *INTERNATIONAL ENERGY AGENCY, IEA*.

Judewicz, M.G., González, S.A., Echeverría, N.I., Fischer, J.R., and Carrica, D.O. (2016). Generalized predictive current control (gpcc) for grid-tie three-phase inverters. *IEEE Transactions on Industrial Electronics*, 63(7), 4475–4484.

Kouro, S., Cortés, P., Vargas, R., Ammann, U., and Rodríguez, J. (2009). Model predictive control—a simple and powerful method to control power converters. *IEEE Transactions on Industrial Electronics*, 56(6), 1826–1838.

Kukrer, O. (1996). Discrete-time current control of voltage-fed three-phase pwm inverters. *IEEE Transactions on Power Electronics*, 11(2), 260–269. doi:10.1109/63.486174.

Marra, E.G. and Pomilio, J.A. (1999). Self-excited induction generator controlled by a vs-pwm bidirectional converter for rural applications. *IEEE Transactions on industry applications*, 35(4), 877–883.

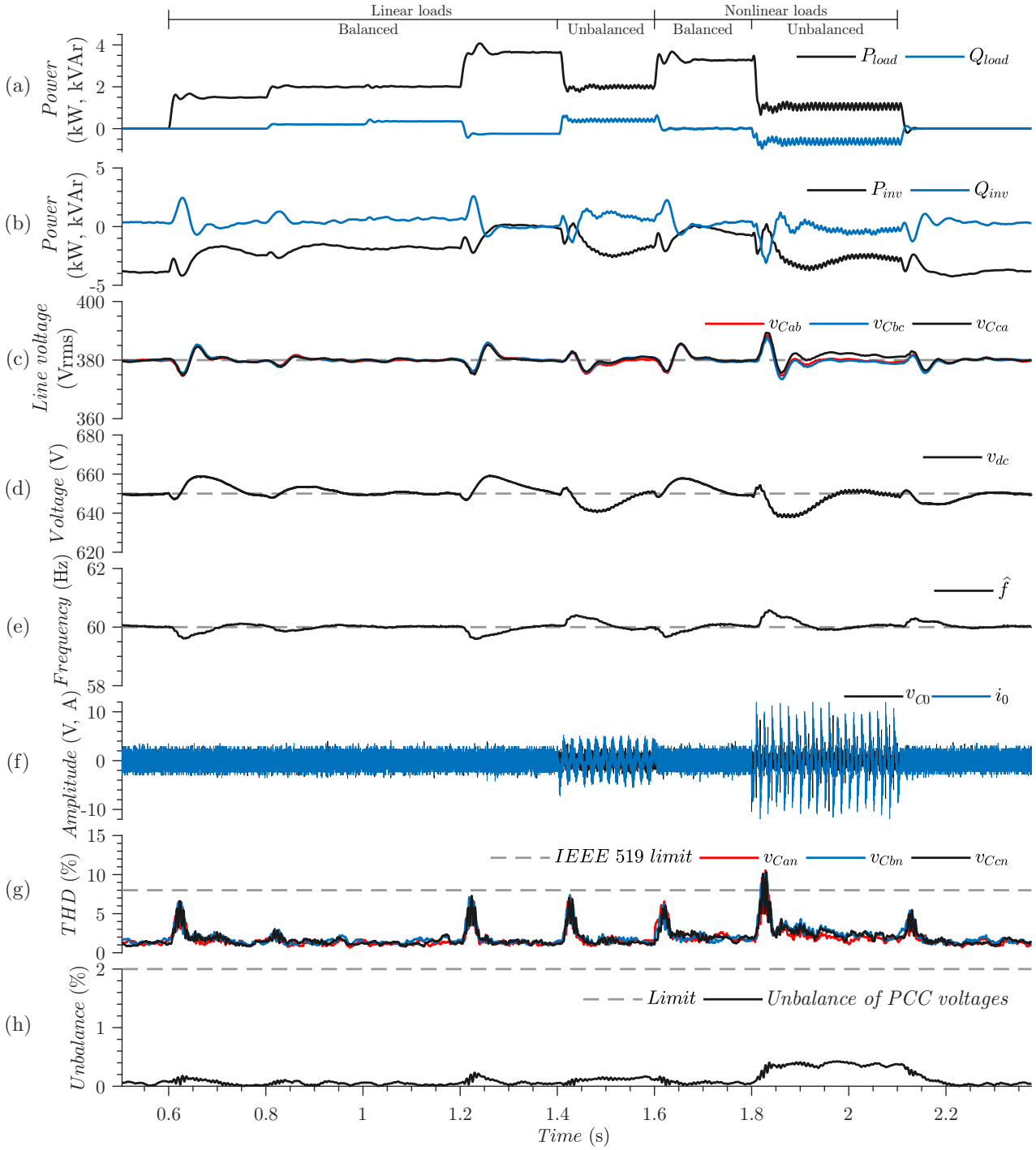

Figure 12. Response of the system to transient load changes: (a) active (P) and reactive (Q) power of load applied; (b) active (P) and reactive (Q) power processed by the inverter; (c) RMS line-to-line voltages at PCC; (d) dc-link voltage; (e) frequency of PCC voltages; (f) zero-axis voltage and current; (g) THD of the phase voltages; (h) voltage unbalance.

Pichan, M., Rastegar, H., and Monfared, M. (2017). Deadbeat control of the stand-alone four-leg inverter considering the effect of the neutral line inductor. *IEEE Transactions on Industrial Electronics*, 64(4), 2592–2601.

Rai, H., Tandan, A., Murthy, S., Singh, B., and Singh, B. (1993). Voltage regulation of self excited induction generator using passive elements. In *1993 Sixth International Conference on Electrical Machines and Drives (Conf. Publ. No. 376)*, 240–245. IET.

Rivera, M., Yaramasu, V., Rodriguez, J., and Wu, B. (2013a). Model predictive current control of two-level four-leg inverters-part ii: Experimental implementation and validation. *IEEE Transactions on Power Electronics*, 28(7), 3469–3478.

Rivera, M., Yaramasu, V., Llor, A., Rodriguez, J., Wu, B., and Fadel, M. (2013b). Digital predictive current control of a three-phase four-leg inverter. *IEEE Transactions on Industrial Electronics*, 60(11), 4903–4912.

Rodriguez, J., Wu, B., Rivera, M., Wilson, A., Yaramasu, V., and Rojas, C. (2010). Model predictive control of three-phase four-leg neutral-point-clamped inverters. In *The 2010 International Power Electronics Conference - ECCE ASIA*, 3112–3116.

Scherer, L.G., Tambara, R.V., and de Camargo, R.F. (2016). Voltage and frequency regulation of standalone self-excited induction generator for micro-hydro power generation using discrete-time adaptive control. *IET Renewable Power Generation*, 10(4), 531–540.

Singh, B. and Kasal, G.K. (2008). Solid state voltage and frequency controller for a stand alone wind power generating system. *IEEE Transactions on Power Electronics*, 23(3), 1170–1177.

Vazquez, S., Rodriguez, J., Rivera, M., Franquelo, L.G., and Norambuena, M. (2017). Model predictive control for power converters and drives: Advances and trends. *IEEE Trans. on Ind. Electron.*, 64(2), 935–947.

Yaramasu, V., Rivera, M., Narimani, M., Wu, B., and Rodriguez, J. (2014). Model predictive approach for a simple and effective load voltage control of four-leg inverter with an output *lc* filter. *IEEE Transactions on Industrial Electronics*, 61(10), 5259–5270.